Engineering Geology 246 (2018) 233–244

Contents lists available at ScienceDirect

Engineering Geology

journal homepage: www.elsevier.com/locate/enggeo

Collaborative 3D geological modeling analysis based on multi-source data standard

Qi Zhang[a,*], Hehua Zhu[b]

[a] Department of Civil and Environmental Engineering, Stanford University, Stanford, CA 94305, USA
[b] Department of Geotechnical Engineering, Tongji University, 1239 Siping Road, Shanghai 200092, PR China

ARTICLE INFO

Keywords:
Multi-source data standard
Collaborative geological modeling analysis
Kriging interpolation
Data integration
iS3

ABSTRACT

A multi-source data standard must be established to reconcile all available geological data such as borehole data, geological mapping data, and rock property data for building a reliable 3D geological model. In addition, a methodology that considers various available data must be developed to provide accurate results that are easy to interpret and convenient for post-modeling analysis. This paper presents a collaborative analysis approach for geological body modeling using multi-source geological data and interpolation theories in different stages and at different places. This approach aims to provide a detailed and comprehensive description and analysis of data, with emphasis on processing flow. The proposed approach contains three major components: establishment of geological databases based on the multi-source data standard to incorporate borehole, geological mapping and rock property data; Combined Kriging interpolation method for data processing; geological algorithms to build, visualize, and post-analyze the 3D geological model. The model integrates multi-source information and is a representative of the geological context. The proposed method is validated by applying it to the Ma-luan mountain tunnel project in Guangdong province, China.

1. Introduction

Building a 3D geological model of geological bodies from geological data is a necessary task in tunnel design, construction, management, and maintenance. A 3D geological model allows companies to make construction plans and prepare for foreseeable dangers. However, in many tunnel projects to date, this task is not executed effectively because of outdated data storage mechanisms, non-uniform data standards, and lack of local updating analysis. Thus, a reliable 3D model must be established using a unified data standard to reconcile all available geological data (De Rienzo et al., 2008; Fasani et al., 2013; Kaufmann and Martin, 2008; Lindsay et al., 2012). Such data include borehole, geological mapping, and rock property data. Furthermore, the model should be imported or visualized via an underground engineering digital platform so that any new local geological information such as monitoring data of tunnel excavation face and geological sketches (Li et al., 2013), can be included to update the original model (Zhu and Li, 2007). This 3D geological modeling technology is characterized by clarity, precision, robustness, and abundance of information (Shao et al., 2011).

The Industry Foundation Class (IFC) data standard (buildingSMART, 2015) is one of the most acceptable tools for data standardization. This data standard was developed by buildingSMART to facilitate interoperability in the architecture, engineering, and construction industries. The standard covers almost every field of civil engineering, with several hundred entities organized into an object-based inheritance hierarchy that comprises the Resource, Core, Interoperability, and Domain layers. The main drawback of this data standard is that it lacks comprehensive object or entity sets for specific fields, such as geology.

To manage geological field data, the Association of Geotechnical and Geoenvironmental Specialists proposed a different data model framework, the AGS framework (Association of Geotechnical and Geoenvironmental Specialists, 2017). This framework facilitates data transmission in geotechnical engineering with unique and easy codes, thereby decreasing the time for data exchange. Moreover, this framework is not fixed and can be adjusted based on individual situations and tunnel construction project demands, as long as they comply with the AGS file format.

Various data structures and interpolation methods (Lam, 1983) have been proposed to achieve 3D geological modeling; the spatial data model is one of the core technologies of 3D geological modeling (Xu et al., 2013). Jones (1988) introduced the concept of geological modeling; since then, data structure and interpolation methods have been

* Corresponding author.
E-mail addresses: qzhang94@stanford.edu (Q. Zhang), zhuhehua@tongji.edu.cn (H. Zhu).

https://doi.org/10.1016/j.enggeo.2018.10.001
Received 11 October 2017; Received in revised form 28 September 2018; Accepted 1 October 2018
Available online 03 October 2018
0013-7952/

investigated extensively. Li et al. (1996) concluded that the typical data structures in geological modeling are grid, triangulated irregular network (TIN), octree, and needle structures. Other data structures are applicable under specific conditions. Wang (2004) established a 3D surface-cylinder data structure that considers the property of the rock. Dong (2013) presented a quasi tri-prism data structure that can be used in digital mine. Among these data structures, TIN data structure is the most popular because the geometric surface of the geological body can be built by estimating elevations of vertices in the whole triangular network. Considering the uncertainty of geological models, scholars have often used geostatistical interpolations (Chilès et al., 2004), such as the Kriging interpolation (Oliver and Webster, 1990). Li et al. (2009) used the Ordinary Kriging (OK) interpolation to generate a stratum model, but this method could not deal with the phenomenon of stratal pinch-out. Kaufmann and Martin (2008) presented a methodology for processing multi-source geological information on a system architecture formed by GIS, GOCAD, and Database. Calcagno et al. (2008) and Guillen et al. (2008) developed a 3D geological modeling method based on the 3D potential-field scalar function and geological rules. This potential-field function contains information, such as geological interfaces, and a function discontinuity represents faults. The geological rules are used to merge separate geological series and in Part II (Guillen et al., 2008), a 3D inverse method is used to validate the models. Zhu et al. (2012) proposed an adapted and automatic Borehole-Surface-Solid method to construct discontinuous geological surfaces induced by missing strata from borehole data. Li et al. (2013) divided geological data into hard data (borehole data) and soft data (geological profiles). These two types of data can then be integrated by Bayesian maximum entropy (BME) nonlinear estimation and Bayesian inference (BI) methods. Touch et al. (2014) conducted 3D geological modeling of geological structures in Phnom Penh subsoils using the Groundwater Modeling System (GMS). However, these proposed approaches are not based on a uniform data standard, and no digital platform is available to visualize the 3D model in the entire building process.

This research study was motivated by the four deficiencies identified in the geological modeling of mountain terrain in road tunnel projects: (1) A multi-source data standard is important in 3D geological modeling in order to incorporate various data into a single geological model and share data with other companies involved in the tunnel project. (2) The model building process should be described in detail, rather than only introducing the theory and displaying the results. (3) The lack of a digital platform in the engineering process means that few benefits are derived from the model. (4) A 3D geological model should be capable of dealing with the phenomenon of stratal pinch-out using numerical methods, such as Indicator Kriging (IK) interpolation.

This paper introduces typical data sources for geotechnical engineering projects, and the proposed multi-source data standard is described thoroughly in Section 2. Details of the proposed modeling framework are discussed in Section 3, which considers the overall framework including the modeling process and six key steps, while Section 4 focuses on the innovative characteristics and some improvements of our framework. In Section 5, we demonstrate an application of our framework to build a 3D geological model for Shenzhen's geotechnical engineering project. Finally, the conclusions are provided in Section 6.

2. Multi-source data standard

2.1. Typical data sources

Given that some geological phenomena are characterized by complexity and uncertainty, the corresponding geological data are heterogeneous (Wu et al., 2005). In geotechnical engineering, various data are classified into three types based on acquisition and usage of information: borehole data, geological mapping data, and property data; the key points are outlined in the following paragraph.

At present, borehole data is the most effective means to build 3D geological models (Meng, 2006; Zhu et al., 2003) or solid models with minimal user intervention (Lemon and Jones, 2003). However, given that drilling boreholes is extremely expensive, and some road tunnels are extremely long, the borehole distribution is sparse. Therefore, geophysical prospecting techniques are often adopted to generate supplementary geological profiles; geological inference results, such as fault zones, are added according to engineering experience. Typical geological profiles include cross-section profiles, exploration point layout plans and topographic-geological profiles. Rock property data, mainly comes from laboratory or in-situ experiments on borehole samples. Both geological mapping data and property data are considered essential supplementary data for any reliable 3D geological modeling.

2.2. Detailed data standard

In the realm of standardization of modeling data, previous research focused on the design of data standards and code systems for borehole data. For example, one standard form of borehole data was suggested and implemented in a web-based GIS system (Chang and Park, 2004). However, this data standard cannot reconcile all the geological information required for our road tunnel project, such as geological mapping data. The variety in borehole information is also insufficient for 3D geological modeling. In addition, this data standard is not based on the AGS data framework but rather suggested by the Korea Institute of Construction Technology (KICT) and thus may not be applicable in other countries.

In this paper, following the AGS file format, we build a simplified but practical version of the data standard with respect to the engineering geology of a road tunnel. This standard contains the following four data groups: a fundamental data group, a borehole data group, a geological mapping data group, and a rock property data group.

2.2.1. Fundamental data group

The fundamental data group provides the basic project information (PROJ), the data units used (UNIT), the data types used (TYPE), and the engineering file transfer information (TRAN). Based on the format of the AGS file, these data groups are defined in Tables 1–4.

2.2.2. Borehole data group

The term borehole includes not only real boreholes but also virtual boreholes; virtual boreholes will be further discussed in Section 3, but in this section, we do not differentiate between them because they have the same data format.

In general, we obtain the (X, Y, Z) coordinates of borehole points. Owing to the heterogeneous geologic conditions and limitations of construction technology, the borehole axis cannot be a straight vertical line but an inclined curve. In engineering practice, clinometers are installed along the borehole axis to obtain additional data for describing the shape of the axis.

Based on the format of the AGS file, the data group is provided in Tables 5–8.

Table 1
Definition of PROJ data subgroup.

Heading	Unit	Type	Description
PROJ_ID	“”	ID	Identifier
PROJ_NAME	“”	X(String)	Project name
PROJ_LOC	“”	X	Project location
PROJ_CLIENT	“”	X	Project client
PROJ_CONT	“”	X	Project contractor
PROJ_ENG	“”	X	Project engineer
PROJ_SIT	“”	X	Project situation
FILE	“”	X	Related file

Table 2
Definition of UNIT data subgroup.

Heading	Unit	Type	Description
UNIT_UNIT	“”	X	Unit of data
UNIT_DESC	“”	X	Description of data

Table 3
Definition of TYPE data subgroup.

Heading	Unit	Type	Description
TYPE_TYPE	“”	X	Data type code
TYPE_DESC	“”	X	Description of data

Table 4
Definition of TRAN data subgroup.

Heading	Unit	Type	Description
TRAN_ISNO	“”	X	Serial number of file
TRAN_DATE	yyyy-mm-dd	DT	Time of transferring file
TRAN_PROD	“”	X	File sender
TRAN_STAT	“”	X	Status of file
TRAN_DESP	“”	X	Description of file
TRAN_AGS	“”	X	AGS serial number
TRAN_RECV	“”	X	File receiver
TRAN_DLIM	“”	X	Data delimiter
TRAN_CONN	“”	X	Data connector

Table 5
Definition of borehole point data subgroup.

Heading	Unit	Type	Description
ID	“”	ID	Identifier of borehole
NAME	“”	X(String)	Name of borehole
X	m	2DP	X coordinate
Y	m	2DP	Y coordinate
Z	m	1DP	Elevation
SECTION_NO	“”	X	Cross-section number

Table 6
Definition of inclination data subgroup.

Heading	Unit	Type	Description
ID	“”	ID	Identifier of inclination point
HOLE_ID	“”	ID	Identifier of borehole
DEPTH	m	2DP	Depth of inclination point
ZENITH	°	0DP	Zenith of inclination point
AZIMUTH	°	0DP	Azimuth of inclination point

Table 7
Definition of axis point data subgroup.

Heading	Unit	Type	Description
ID	“”	ID	Identifier of axis point
HOLE_ID	“”	ID	Identifier of borehole
X	m	2DP	X coordinate of axis point
Y	m	2DP	Y coordinate of axis point
SECTION_NO	“”	X	Cross-section number
STRATUM_NO	“”	X	Downward stratum number

2.2.3. Geological mapping data group

In GIS, the ideal model to store geological mapping data is the vector data model. As in other data models and structures, the vector data model consists of spatial and property data, which are mutually connected by a unique identifier (ID).

For the vector data model, the storage mechanisms differ depending on the existence of topological relationships (Tables 9–12). In practice, for exploration point layout plan, we do not consider the topological relationship. By contrast, for topographic-geological profiles and cross-section profiles, the topological relationship between strata is extremely important. Based on the format of the AGS file, the data group is provided as follows: the vector data model with topological relationships is given in Tables 9–11, and the vector data model without topological relationships (always referred as the noodle data model) is presented in Table 12.

Table 8
Definition of stratum data subgroup.

Heading	Unit	Type	Description
ID	“”	ID	Identifier of stratum
STRATUM_NO	“”	X	Stratum number
HOLE_ID	“”	ID	Identifier of borehole
D_FROM	m	1DP	Stratum initial elevation
D_TO	m	1DP	Stratum end elevation
NAME	“”	X	Name of rock

Table 9
Definition of node data subgroup.

Heading	Unit	Type	Description
NODE_ID	“”	ID	Identifier of node
X	m	2DP	X coordinate of node
Y	m	2DP	Y coordinate of node
Z	m	2DP	Z coordinate of node
RELATED ARC_ID	“”	ID_array	Related identifiers of arc of same node

Table 10
Definition of arc data subgroup.

Heading	Unit	Type	Description
ARC_ID	“”	ID	Identifier of arc
START NODE_ID	“”	ID	Identifier of arc starting node
END NODE_ID	“”	ID	Identifier of arc ending node
MID NODE_ID	“”	ID_array	Identifier of arc middle nodes
LEFT POLYGON_ID	“”	ID	Identifier of left polygon
RIGHT POLYGON_ID	“”	ID	Identifier of right polygon

Table 11
Definition of polygon data subgroup.

Heading	Unit	Type	Description
ID	“”	ID	Identifier of polygon
RELATED ARC_ID	“”	ID_array	Related identifiers of arc of same polygon

Table 12
Noodle data structure.

Character	ID	Coordinate
Node	*	(X coordinate, Y coordinate, Z coordinate)
Arc	*	Coordinate array: (X1, Y1, Z1) (X2, Y2, Z2) … (Xn, Yn, Zn)
Polygon	*	Coordinate closed loop: (X1, Y1, Z1) (X2, Y2, Z2) … (Xn, Yn, Zn) … (X1, Y1, Z1)

2.2.4. Rock property data group

Unlike the Phnom Penh subsoils study (Touch et al., 2014), our data group does not distinguish the physical properties from the engineering properties. Although more complex relationships have been shown between the geological structure field and the property parameter field (Zhu et al., 2013), our data group only considers the simple case; in other words, each property data record has its own unique identifier

Table 13
Definition of rock property data group.

Heading	Unit	Type	Description
ID	""	ID	Identifier of borehole
S_DEPTH	m	2DP	Sample depth
W_STATE	""	X	Water state
S_HEIGHT	mm	1DP	Sample height
S_DIAMETER	mm	1DP	Sample diameter
N_DENSITY	g/m^3	2DP	Natural density
S_DENSITY	g/m^3	2DP	Saturated density
W_ABSORPTION	%	2DP	Water adsorption
C_STRENGTH	MPa	1DP	Compression strength
D_MODULUS	GPa	2DP	Dynamic Young's modulus
S_MODULUS	GPa	2DP	Static Young's modulus
P_RATIO	""	2DP	Poisson's ratio
I_ANGLE	°	1DP	Internal friction angle
COHESION	MPa	1DP	Cohesion
L_VELOCITY	m/s	0DP	Longitudinal wave velocity
S_VELOCITY	m/s	0DP	Shear wave velocity
I_COEFFICIENT	""	2DP	Coefficient of integrity
D_INTEGRITY	""	X	Degree of integrity
INTENSITY_R	nC/kg·h	2DP	Average intensity of radioactivity
EQUIVALENT_U	0.01%eU	2DP	Equivalent content of uranium
SIGMA_H	MPa	1DP	Max horizontal principle stress
SIGMA_h	MPa	1DP	Min horizontal principle stress
SIGMA_Z	MPa	1DP	Self-weight stress
LAMBDA	""	1DP	Lateral pressure coefficient

(ID). Based on the format of the AGS file, the data group is given in Table 13.

2.3. Discussion

Fault data can be organized into our proposed data standard because, firstly, the rock properties in the fault region can be recovered from the rock property data group. Secondly, although the stratum sequence in the fault region might change, the borehole data group is still valid in the fault region. Finally, the position of the fault plane comes from geological inference and is reflected in the geological profiles; therefore, the geological mapping data group can be applied.

The above-defined data groups and subgroups are not independent but rather correlated with one another. The inherent relationship in the borehole data group is shown in Fig. 1; the coordinates of the axis points are calculated from the borehole point data, the inclination data, and the geological mapping data (Fig. 2). The interaction between these data groups and 3D geological modeling is detailed in Section 3.

3. General framework of collaborative 3D geological modeling analysis

A novel modeling framework is proposed to improve the accuracy of the 3D geological model based on a suggested multi-source data standard and integration of all types of geological data. The conceptual workflow of the collaborative 3D geological modeling analysis procedure is outlined in Fig. 2. The implementation can be decomposed into six key steps, and step-by-step execution is explained in detail below.

3.1. Pre-processing analysis of fundamental geological modeling data

The fundamental geological modeling data comes from various sources and therefore it is necessary to perform a refining (integration) process to eliminate abnormal information and render the data as consistent as possible. The aim here is to develop a representative lithological section, in other words, to identify the rock (stratum) type in each place; to achieve this we use some techniques in statistical learning.

Firstly, the lithological information and rock properties information are divided into several categories. For example, the lithological information includes the grain size, color and mineralogy; while the rock properties are the strength, Young's modulus, and hardness. Each category is one covariate and we include both qualitative and quantitative covariates in our statistical learning model. It should be noted that for the lithological information, we double the number of covariates since the lithology in boreholes is recorded at interval of tens of centimeters, but it is recorded at a much larger interval in geological profiles. In order for our model to better utilize the precise information from borehole data, we have incorporated 'covar_bore, covar_geophy'. The covariates of rock properties mainly come from borehole data, so there is no need to double them.

Using the borehole logs and geological profiles we can extract the corresponding covariates for each location, which gives us a data matrix X_{test} of size n_{test} by p, where p is the total number of categories and n_{test} is the total number of locations where we want to identify the rock type. In locations where there is no borehole, some 'covar_bore' covariates will have missing values.

This data extraction procedure is repeated on previous, but similar, engineering projects and using data from geotechnical engineering handbooks or specifications; comparison with these sources will give the output (rock type) and our training matrix X_{train} of size n_{train} by p.

The K-MART gradient boosting tree algorithm (Friedman, 2001; Hastie et al., 2009; James et al., 2013) (k class multiple additive regression tress) is then run on the training matrix with parameters chosen by cross validation to make predictions on the test matrix for every location; the result is our representative lithological section. This technique allows us to recognize important variables from partial dependence plots (Friedman, 2001).

The reason for choosing a gradient boosting tree is that it has inherited advantages: Firstly, it can naturally handle any missing values; secondly, it has an internal variable subset selection mechanism, and finally, it is robust to irrelevant inputs.

From the above representative lithological section, the boundaries of the various strata can be identified, and a comprehensive regional stratigraphic sequence table can be compiled. In this table, by convention, the serial number of the newest stratum is 1, and the larger numbers represent older strata. This table also serves as a criterion for stratum locations in 3D geological modeling. This table can be used to express borehole information in a binary topology structure from the ground surface to the underground subsurface. Fig. 3 shows the simple

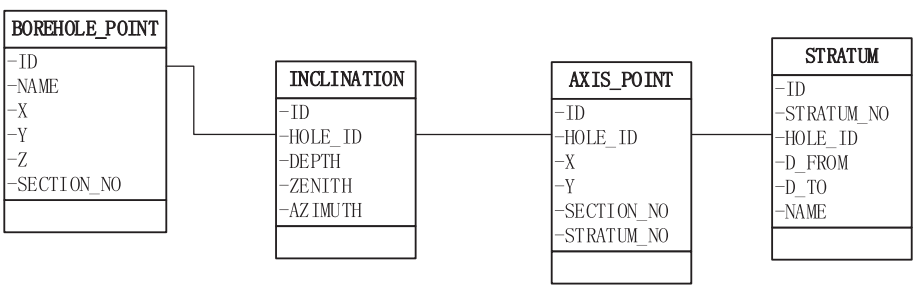

Fig. 1. Inherent relationship in borehole data group.

Data standard is used to store data, data integration is based on the stored data, and integrates real borehole data and virtual borehole data obtained from geological profiles, to obtain representative lithological section. Kriging is then applied on this RLS.

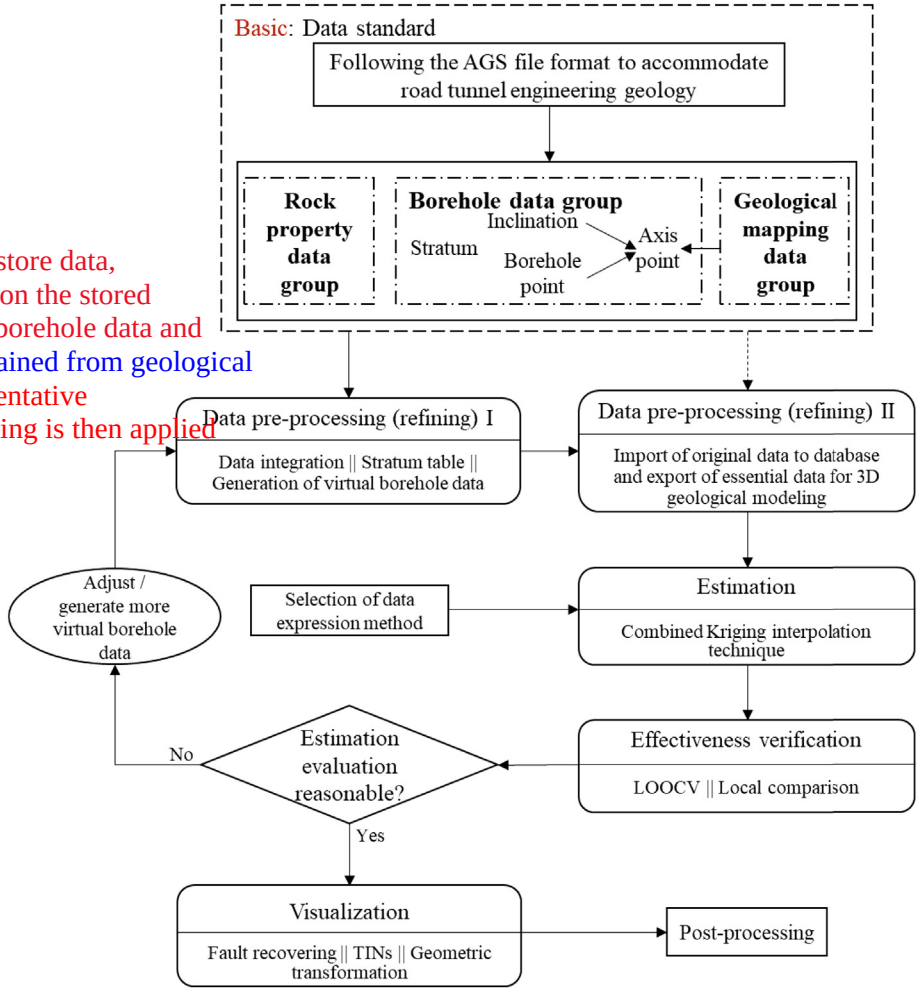

Fig. 2. Conceptual workflow of 3D geological modeling procedure.

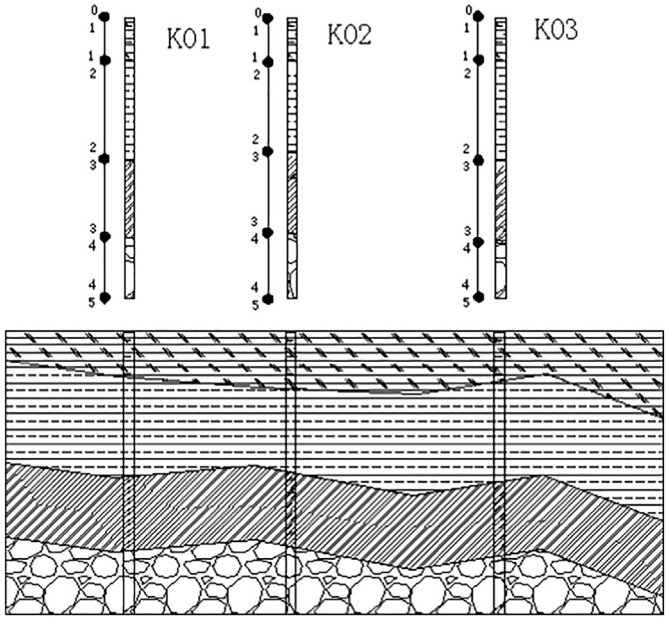

Fig. 3. Sketch of binary topology structure from borehole data.

schematic diagram for the binary topology structure.

The geological profiles can also be used to generate virtual borehole data. As we know, borehole distribution is sparse in engineering practice because of the expense of drilling; thus, we adopt the idea of virtual borehole to increase the input data as well as offset the lack of original data. The virtual borehole can be produced in two ways, either from known regions with geological profiles or from geological inference (Zhu et al., 2006). We then incorporate this newly created virtual borehole data into our original borehole data sets for future use. In addition, the use of a virtual borehole can be interpreted as a bridge to connect geological mapping data with real borehole data to increase the accuracy of the model.

Finally, based on the established multi-source data standard, we import all the data into the database. Any data required is exported from the database by SQL statements and are stored in Excel.

3.2. Selection of data expression method

Two types of data structure are used in this framework. The triangulated irregular network (TIN) data structure is used to generate the stratum surface, and the construction solid geometry (CSG) data structure is used to construct the geological body by geometric transformation and Boolean operation.

3.3. Estimation of stratum thickness using Combined Kriging technique

Using the extracted geological data of Section 3.1, the Combined

Kriging method is applied to estimate the thickness in the triangle network. Before we introduce this method, we need to review some basic properties and equations in the Kriging interpolation method.

In geological modeling, sample data, such as borehole data, are interpreted as the result of a random process. The Kriging method can be used to build a methodological basis for the spatial inference of quantities in unobserved locations and quantify the estimation error (Oliver, 2010; Trangmar et al., 1986); this method is more reasonable than piece-wise polynomial spline fitting or linear regression.

We use a regionalized random variable $Z(\tilde{\boldsymbol{x}})$ to represent this homogeneous random process. Some reasonable assumptions are necessary to proceed with our spatial inference; in this framework, we assume that the first moment of $Z(\tilde{\boldsymbol{x}})$ is stationary. The covariance and semivariogram between two regionalized random variables $Z(\tilde{\boldsymbol{x}})$ and $Z(\tilde{\boldsymbol{x}} + \tilde{\boldsymbol{h}})$ depend solely on the spatial distance $\|\tilde{\boldsymbol{h}}\|_2$ between them. Probability theory indicates the relationship between the covariance function and semivariogram (Oliver, 2010), which is given as

$$C(\|\tilde{\boldsymbol{h}}\|_2) = C(0) - \gamma(\|\tilde{\boldsymbol{h}}\|_2) \tag{1}$$

where $C(\blacksquare)$ is the covariance function between two random variables, $C(0)$ is the variance of $Z(\tilde{\boldsymbol{x}})$ itself, and $\gamma(\blacksquare)$ is the semivariogram.

Spatial estimation of the average value for the regionalized random variable $Z(\tilde{\boldsymbol{x}})$ in an infinitesimal neighborhood of an unobserved location $\tilde{\boldsymbol{x}}_0$ is always calculated from the weighted linear combination of observed values, as shown in Eq. (2):

$$\hat{Z}(\tilde{\boldsymbol{x}}_0) = \sum_{i=1}^{n} \lambda_i z(\tilde{\boldsymbol{x}}_i) \tag{2}$$

where $\hat{Z}(\tilde{\boldsymbol{x}}_0)$ is the spatial estimate at location $\tilde{\boldsymbol{x}}_0$; $\lambda_i (1 \le i \le n)$ is the weight coefficient; $z(\tilde{\boldsymbol{x}}_1)$, $z(\tilde{\boldsymbol{x}}_2)$, $z(\tilde{\boldsymbol{x}}_3)$, ..., $z(\tilde{\boldsymbol{x}}_n)$ are the observed values of $Z(\tilde{\boldsymbol{x}})$ at n different locations. We then derive the explicit expression for estimate variance σ_E^2 using calculus procedure,

$$\sigma_E^2 = \mathrm{Var}[\hat{Z}(\tilde{\boldsymbol{x}}_0) - Z(\tilde{\boldsymbol{x}}_0)] = 2\sum_{i=1}^{n} \lambda_i \gamma(\|\tilde{\boldsymbol{x}}_0 - \tilde{\boldsymbol{x}}_i\|_2) - \sum_{i=1}^{n}\sum_{j=1}^{n} \lambda_i \lambda_j \gamma(\|\tilde{\boldsymbol{x}}_i - \tilde{\boldsymbol{x}}_j\|_2) - \gamma(0+0) \tag{3}$$

where $\mathrm{Var}(\blacksquare)$ is the variance, $Z(\tilde{\boldsymbol{x}}_0)$ is the average value of $Z(\tilde{\boldsymbol{x}})$ in an infinitesimal neighborhood of an unobserved location $\tilde{\boldsymbol{x}}_0$, $\gamma(0+0) = \lim_{x \to 0^+} \gamma(x)$ is the right limit of the semivariogram at the origin (the nugget effect). Some studies ignore the last term in their formulae.

In the Kriging method, weighted coefficients are calculated to render the estimate unbiased and minimize the estimate variance (Oliver and Webster, 1990), which is known as the Kriging equation as follows (where $1 \le i \le n$):

$$\begin{cases} \sum_{j=1}^{n} \lambda_j \gamma(\|\tilde{\boldsymbol{x}}_i - \tilde{\boldsymbol{x}}_j\|_2) + \mu = \gamma(\|\tilde{\boldsymbol{x}}_0 - \tilde{\boldsymbol{x}}_i\|_2) \\ \sum_{j=1}^{n} \lambda_j - 1 = 0 \end{cases} \tag{4}$$

After solving this equation, we use Eq. (2) to obtain the value of $\hat{Z}(\tilde{\boldsymbol{x}}_0)$. However, when $Z(\tilde{\boldsymbol{x}})$ represents the value of probability between 0 and 1, the above process is known as Indicator Kriging interpolation (IK), otherwise, it is termed Ordinary Kriging interpolation (OK).

In our framework, we developed a Combined Kriging (CK) interpolation algorithm to deal with the phenomenon of stratal pinch-out. The combined algorithm uses IK and OK methods simultaneously and is an analogy to the approach that solves the problem in mineralogy, where several different mineralization mechanisms occur at the same location. To clearly describe this algorithm, here $P(\tilde{\boldsymbol{x}})$ denotes the probability of the existence of a specific stratum, which is in interval $[0,1]$; and $p(\tilde{\boldsymbol{x}})$ is the realization of $P(\tilde{\boldsymbol{x}})$ at position $\tilde{\boldsymbol{x}}$, which can only take a value of 0 or 1. All the above operations for $Z(\tilde{\boldsymbol{x}})$ are the same for $P(\tilde{\boldsymbol{x}})$. In the 3D geological modeling process, $Z(\tilde{\boldsymbol{x}})$ now stands for the stratum thickness random variable. Thus, the Combined Kriging interpolation algorithm is provided as follows:

(1) For unobserved location $\tilde{\boldsymbol{x}}_0$, $\hat{P}(\tilde{\boldsymbol{x}}_0)$ is calculated using the IK method;

(2) The set Ω is found such that $\Omega = \{\tilde{\boldsymbol{x}}_i \mid p(\tilde{\boldsymbol{x}}_i) = 1 \ (1 \le i \le n)\}$;

(3) $\hat{Z}(\tilde{\boldsymbol{x}}_0)$ is calculated by the OK Method based only on the value of $z(\tilde{\boldsymbol{x}}_i)$ if $\tilde{\boldsymbol{x}}_i \in \Omega$;

(4) $\hat{Z}(\tilde{\boldsymbol{x}}_0) \times \hat{P}(\tilde{\boldsymbol{x}}_0)$ is calculated; this is the final estimate of the stratum thickness at location $\tilde{\boldsymbol{x}}_0$.

3.4. Effectiveness verification and evaluation of the estimation

Although we have proposed this CK algorithm, we need to further verify its effectiveness (Tacher et al., 2006; Thierry et al., 2009), evaluate the estimated results and make any adjustments.

In our framework, the effectiveness of the CK method is verified in two different ways. The primary method is known as Leave-one-out cross-validation (LOOCV). In LOOCV, we have a sample set that contains output information $z(\tilde{\boldsymbol{x}})$ at n points. For each point, we use information provided by other $n-1$ points to estimate $z(\tilde{\boldsymbol{x}})$ at the current point. Therefore, n pairs of estimated and observed values are obtained (Oliver and Webster, 2015). The mean squared error (MSE) is then computed from these pairs of values using the formula given in Eq. (5) (Liu et al., 2013; Xie et al., 2011):

$$MSE = \frac{\sum_{i=1}^{n} [\hat{Z}(\tilde{\boldsymbol{x}}_i) - z(\tilde{\boldsymbol{x}}_i)]^2}{n} \tag{5}$$

Test error

where $\hat{Z}(\tilde{\boldsymbol{x}}_i)$ is the spatial estimate at location $\tilde{\boldsymbol{x}}_i$ using the left $n-1$ points, $z(\tilde{\boldsymbol{x}}_i)$ is the observed value of $Z(\tilde{\boldsymbol{x}})$ at location $\tilde{\boldsymbol{x}}_i$, and n is the total number of sample points. An effective method should have a low MSE value (Douaik et al., 2005).

Train error The secondary method is the local comparison method; we compare the estimates obtained for the stratum thickness with given data obtained from geological explorations using longitudinal section profiles. A profile is constructed by spline fitting the estimations or given data in the local area.

Next, since we adopt the idea of a virtual borehole. It is necessary to carefully check where the virtual borehole and other indirect data with low precision are used in our original 3D geological model (Zhu et al., 2006). When something unrealistic is found, the virtual borehole data is adjusted or additionally generated to update the estimation of thickness until it is reasonable. These estimated results of the stratum thickness are then added up to obtain the value of stratum surface elevation.

主要和真实钻孔数据比较

3.5. Establishment and display of 3D geological body

In geotechnical engineering, the position of a fault is of vital importance. Therefore, we need to incorporate a fault recovery method (Li et al., 2013; Wu and Xu, 2003) in the 3D geological body modeling process.

Firstly, using geological inference, if a fault zone exists, we need to determine the fault impact area and build a horizontal grid of the area. Then we need to assign elevation values to the grid nodes based on the available information.

Secondly, we need to define the tectonically constrained boundaries. For normal (obverse) and reverse faults, we consider the fault surface as an additional tectonically constrained boundary, while for strike-slip faults, the fault surface is treated as unconstrained.

Thirdly, by using the estimated elevation data and our defined tectonically constrained boundaries, a series of TINs is generated on the nodes of the output grid using a constrained Delaunay triangulation algorithm (fault surface included).

Fourthly, geological bodies are created by geometric transformation

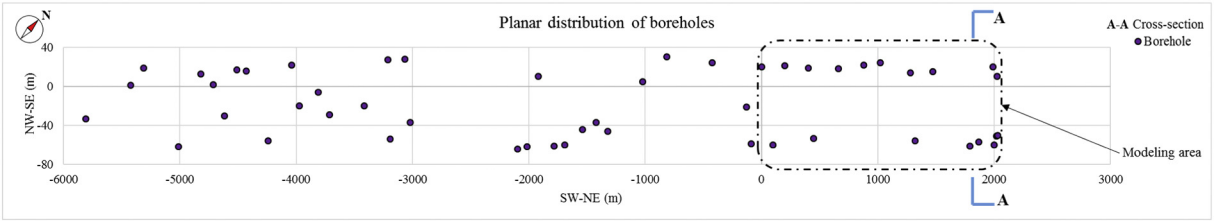

Fig. 4. Planar distribution of boreholes in the Ma-luan road tunnel project.

among TINs based on their topological relationship information (Holden et al., 2003; Lu, 2002), which is stored according to the rule of the geological mapping data group. In this process, we also connect our stratum subgroup with the property data group at prescribed locations through a unique identifier 'Borehole_ID'. A Boolean operation is then conducted to achieve the three-dimensional unity of geological bodies and fault surfaces.

Finally, the whole 3D geological body is displayed so that the rock properties information can be viewed when it is available.

3.6. Post-processing of geological model

Based on the constructed 3D geological model, we can obtain valuable information, such as cross-sectional profiles at any point and the slope of mountain surface, which could provide improved guidance for tunnel construction and maintenance.

4. Characteristics and improvements

Compared with the existing 3D geological modeling and visualization, the characteristics and improvements provided in the proposed modeling framework involve three aspects: Weight assignment, treatment of stratal pinch-out phenomenon, and integration of various dimensional information. The following paragraphs explain these aspects.

In 3D geological modeling, multi-source data does not have uniform precision and resolution; therefore, the weighting must be defined. In the proposed framework, this is achieved in an implicit way. Firstly, in Section 3.1, when different sources of data provide contradictory information for the same place, we rely on the high-resolution data or nearby data, and give low-resolution data a low weighting in gradient boosting tree algorithm. Secondly, in the Combined Kriging interpolation method outlined in Section 3.3, the source that is closest to the test (grid) point will be more reliable and thus have a higher weighting, and vice versa. This pattern is captured by the trend in the semivariogram; in other words, a greater distance will lead to a larger variance and lower weighting. Thirdly, in Section 3.4, we need to check the places where low precision data is used since these will have a lower weight. In contrast, we need not worry about the real borehole data since it is a reflection of the true geological conditions, having high precision and higher weighting.

Our proposed Combined Kriging algorithm can deal with the stratal pinch-out phenomenon because the idea of Indicator Kriging is incorporated into our algorithm; this will be illustrated it in the case study of Ma-luan mountain tunnel project given below.

Another characteristic of our proposed framework is that various dimensional information can be incorporated using multi-source data standards, statistical learning methods and virtual borehole. More specifically, to use geological profiles in 3D geological modeling, we first establish a corresponding data group, making it convenient for data storage, data transmission and data extraction. Then we apply gradient boosting tree algorithm to conclude a representatively lithological section. Following that, virtual borehole will be produced, since virtual borehole and real borehole are both linear type data, we can easily integrate them and calculate the axis point subgroup of the borehole data group. Then we extract data from the database and apply a Combined Kriging algorithm to predict the output value (latitude) at test points. In this way, we can integrate 2D planar data and 1D borehole linear type data.

5. A case study: Ma-luan mountain tunnel project

In this section, we apply our proposed framework to a geotechnical engineering project to generate results and validate our concepts.

5.1. Engineering background and research area

The Ma-luan mountain tunnel is located in the Pearl River Delta, in the eastern section of Shenzhen city, Guangdong province, China. This tunnel is a part of the Ping-yan passage, which is a valuable connection between Pingshan new district and the Yantian district. The tunnel uses the separation mode, instead of a twin-arch mode, with a spacing of 40 m. The length of the left tunnel is 7.899 km, and that of the right tunnel is 7.904 km, from northeast to southwest. The tunnel is categorized as an ultra-long city road tunnel. One shaft and a number of cross-evacuation aisles have been built along the tunnel. The mountain range of the Ma-luan tunnel is a geological body that is mostly comprised of weathered and unweathered granite. Cataclastic rock might also exist and should be investigated during tunnel construction.

In this project, a total of 50 exploration boreholes were drilled, roughly distributed between the left and right tunnels. This borehole distribution is illustrated in Fig. 4. Fifteen cross-section profiles were derived in our study area; for instance, the A–A (see Fig. 4) cross-section profile is shown in Fig. 5. Tables 14 and 15 list some of the experimental results used to determine the rock properties.

In our case study, the right section (2030 m × 95 m) of the geological body was chosen as our research area because of its complex geological conditions, such as a weak layer and stratal pinch-out phenomenon. We choose 18 borehole samples as our primary data sources, as shown in Fig. 4.

5.2. Results of collaborative 3D geological modeling analysis

Following the steps described in Section 3.1, after refining the geological modeling data we produced a regionally stratigraphic sequence table (Table 16) and extracted data. Ten fields are included in the extracted data, and one portion of extracted data is shown in Table 17.

Next, we used the Combined Kriging technique to estimate stratum thickness. In our proposed framework, we assume semivariogram is given; however, in practice, we do not know the expression of the semivariogram in advance. To solve this issue, we propose an approach for obtaining an approximate expression of the semivariogram from the data. First, suppose there are n data points in the data and then calculate the dissimilarity for every data pair. The number of all data pairs should be $\binom{n}{2} = \frac{n(n-1)}{2}$. Second, divide all $\binom{n}{2}$ data pairs into several clusters such that in the $k^{\text{th}}(k \geq 1)$ cluster, the dissimilarity of each data pair is in the interval $[(k-1)d - \epsilon, (k-1)d + \epsilon]$, where d is the lag increment, and ϵ is the error tolerance. In practice, ϵ should be less than one third of the lag increment d, and we should therefore choose an appropriate value for d that is neither too big nor too small so that

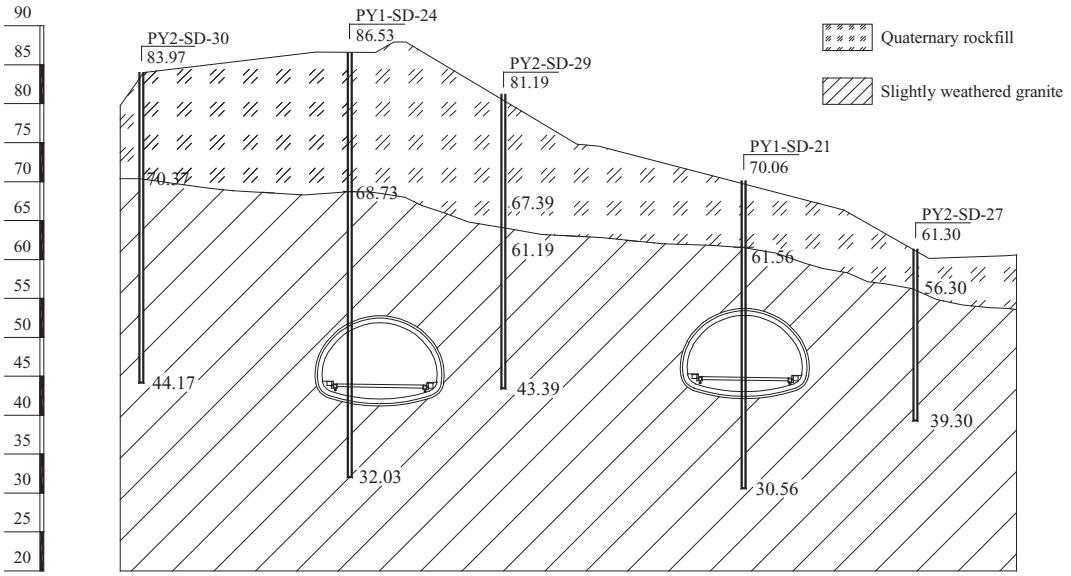

Fig. 5. Geological body transverse cross-section profile (A–A).

Table 14
Some borehole acoustic logging results for a section of the Ma-luan tunnel.

Not used directly

ID	Rock property	Test depth (m)	Longitudinal wave velocity (m/s)	Dynamic Poisson's ratio	Dynamic Young's modulus (GPa)	Static Young's modulus (GPa)	Coefficient of integrity
PY2-SD-10	Slightly weathered	69–102	4311	0.30	35.37	23.28	0.68
PY2-SD-13	Slightly weathered	57–94	4683	0.28	38.85	27.71	0.73
PY2-SD-36	Slightly weathered	76–100	4616	0.29	37.24	25.64	0.71
PY2-SD-39	Slightly weathered	47–81	4760	0.28	40.55	30.78	0.75
PY2-SD-18	Slightly weathered	46–77	4708	0.28	39.29	29.57	0.73
PY2-SD-19	Slightly weathered	37–65	4668	0.28	38.41	27.24	0.72
PY2-SD-22	Slightly weathered	62–81	4450	0.29	33.37	18.96	0.66
	Cataclasite	81–98	3309	0.34	14.10	2.25	0.36
PY2-SD-23	Slightly weathered	25–37	4487	0.29	34.18	21.53	0.67
	Slightly weathered	37–52	4572	0.29	36.08	25.16	0.69
	Cataclasite	52–84	3226	0.34	13.11	1.99	0.34
PY2-SD-42	Slightly weathered	71–105	4764	0.28	40.71	30.98	0.75
PY2-SD-43	Slightly weathered	70–103	4800	0.28	41.57	31.81	0.76

Table 15
Some radioactivity measurements for a section of the Ma-luan tunnel.

Not used directly

	Average intensity of radioactivity (nC/kg·h)	Maximum (nC/kg·h)	Minimum (nC/kg·h)	Equivalent content of uranium (0.01%eU)	Maximum content of uranium (0.01%eU)
PY1-SD-10	5.44	14.72	3.22	0.17	0.50
PY1-SD-15	7.38	9.48	4.75	0.26	0.32
PY1-SD-17	6.71	9.27	4.41	0.22	0.31
Statistics	6.51	14.72	3.22	0.22	0.50

Table 16
Regionally stratigraphic sequence table.

Stratum number	Name of rock
1	Quaternary rockfill
2	Strongly weathered coarse-grained granite
3	Moderate weathered coarse-grained granite
4	Slightly weathered coarse-grained granite
5	Cataclasite

certain data pairs are found in each cluster. For the same k^{th} cluster, we can estimate the value of the semivariogram (the 'hat' symbol means estimation) at a distance $(k-1)d$ by using Eq. (6),

$$\hat{\gamma}_{(k-1)d} = \frac{1}{2N(k)} \sum_{i=1}^{N(k)} [z(\tilde{\boldsymbol{x}}_{i,1}) - z(\tilde{\boldsymbol{x}}_{i,2})]^2 \tag{6}$$

where $z(\tilde{\boldsymbol{x}})$ is one output field of the data such as stratum thickness or the probability of the existence of one stratum, $N(k)$ is the total number of data pairs in this cluster. By definition, we know that $\sum_{k\geq 1} N(k) = \binom{n}{2}$. The same operation is repeated for each cluster. Finally, we obtain a scatter diagram of the semivariogram for this output field, which is also called an empirical semivariogram. From the empirical semivariogram, the range, nugget, sill of the semivariogram model could be determined in following way.

Here, the weighted least square method proposed by Cressie (1985) is adopted. This method tries to minimize the weighted residual sum of squares (WRSS) with respect to three unknowns: range a, nugget C_0, and sill C_s. In the paper of Lamorey and Jacobson (1995), the formula

Table 17
One portion of extracted data from stratigraphic sequencing.

Sample	Field								
	ID	X	Y	Z	T.S.1[a]	T.S.2	T.S.3	T.S.4	T.S.5	T.S.4
1	PY2-SD-19	1.00	20.00	141.8	0.0	4.6	10.2	50.4	0.0	76.6
2	PY2-SD-20	200.00	21.00	229.6	0.0	6.2	9.3	70.4	0.0	143.6
3	PY2-SD-43	400.00	19.00	261.0	0.0	5.1	11.4	86.7	0.0	157.7
4	PY2-SD-21	660.00	18.00	186.8	0.0	7.2	14.0	74.8	0.0	90.8
5	PY2-SD-17	880.00	22.00	205.6	0.0	6.2	9.3	117.1	0.0	73.0
6	PY2-SD-45	1020.00	24.00	227.0	0.0	5.2	10.5	129.4	7.0	75.0
7	PY2-SD-22	1280.00	14.00	203.0	0.0	6.2	12.2	62.7	17.5	104.4
8	PY2-SD-23	1470.00	15.00	175.0	0.0	5.1	9.3	37.3	32.0	91.3
9	PY2-SD-24	1990.00	20.00	84.0	9.0	0.0	0.0	29.0	0.0	46.0
10	PY2-SD-21	2025.00	10.00	73.0	13.0	0.0	0.0	14.6	0.0	45.4

[a] T.S.N – Thickness of stratum # N.

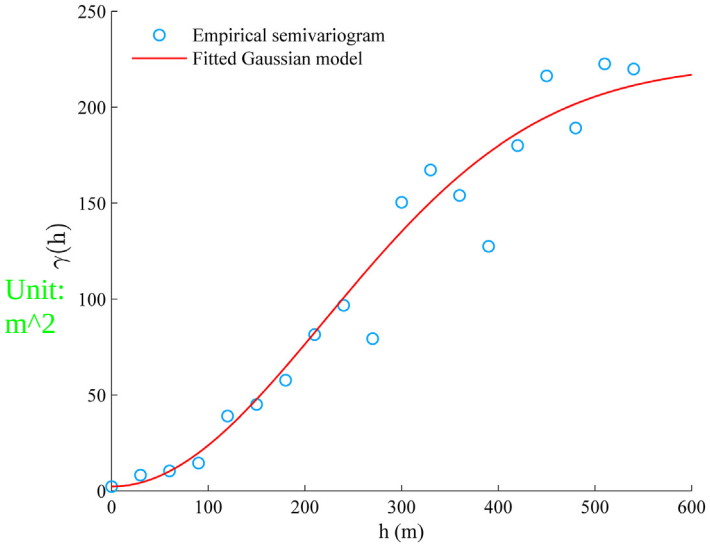

Fig. 6. Semivariogram of cataclasite stratum thickness.

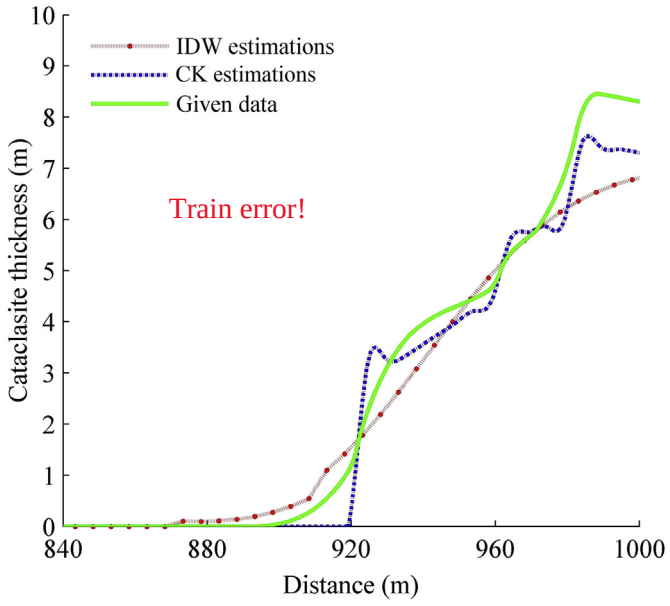

Fig. 8. Local comparison among two interpolation curves and given data curve.

for WRSS is given by:

$$WRSS(a, C_0, C_s) = \frac{N(1)}{C_0^2}[\hat{\gamma}(0) - C_0]^2 + \sum_{k=2}^{T_m} \frac{N(k)}{\gamma^2(h_k; a, C_0, C_s)}[\hat{\gamma}(h_k) - \gamma(h_k; a, C_0, C_s)]^2 \quad (7)$$

where $h_k (k \geq 1)$ equals $(k-1)d$ and d is the lag increment, $\hat{\gamma}(h_k)$ is the single point in the empirical semivariogram defined in Eq. (6), $\gamma(h_k; a, C_0, C_s)$ is the selected theoretical semivariogram model, such as the Gaussian model or spherical model, $N(k)$ is the same as in Eq. (6), T_m is the number of clusters over which the semivariogram will be calculated. The expressions for the Gaussian model and spherical model can be found in Devi et al. (2009) and Sakata and Ashida (2011). We next take the derivative of WRSS and set it to zero, which gives a non-linear system of equations. Newton's method is then applied to find the roots, which are the optimal values for the range, nugget, and sill. In practice, the range is consistently in the interval from 100 m to 1000 m. Fig. 6 shows the empirical semivariogram of the cataclasite stratum thickness; by using the above approach, we obtain the following parameters of the Gaussian semivariogram model: range is 540m; nugget is 2.25m^2; sill is 222.25m^2. Ordinary Kriging的参数

After determining the expressions for all the semivariograms, we can apply the Combined Kriging technique to estimate each stratum thickness in MATLAB. Here we display the results for the cataclasite stratum since it is one of the primary engineering concerns in the construction process (Fig. 7). Then we proceed to verify the effectiveness of the CK technique and evaluate the estimations.

To achieve this, another interpolation technique is used, the Inverse Distance Weighted (IDW) method, and compared with CK method. In LOOCV, the MSE for CK is 1.3m^2 while for IDW it is 12.8m^2, which

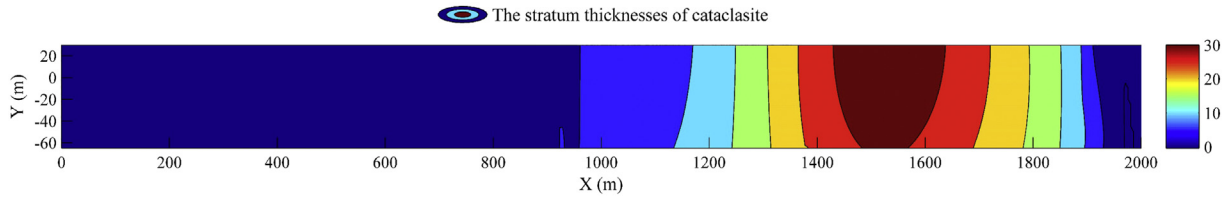

Fig. 7. Estimate of cataclasite stratum thicknesses.

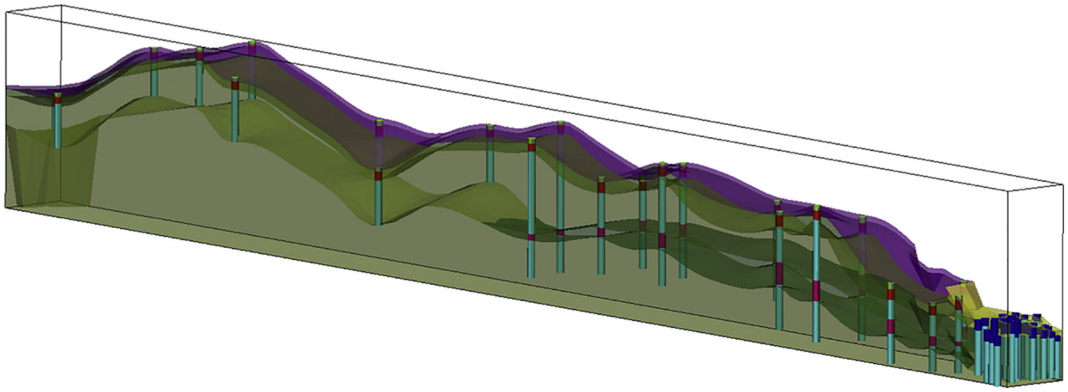

Fig. 9. TINs of all stratum surfaces.

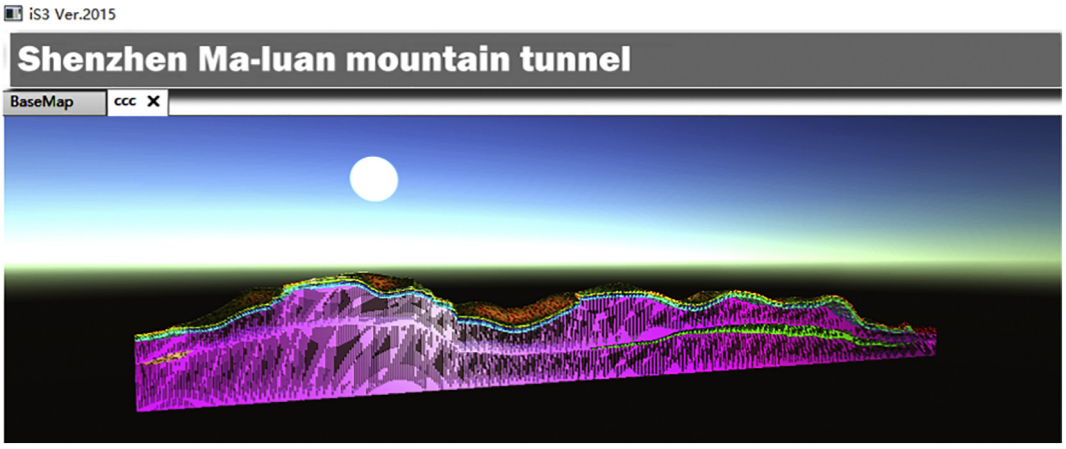

Fig. 10. Final 3D geological model on iS3 platform.

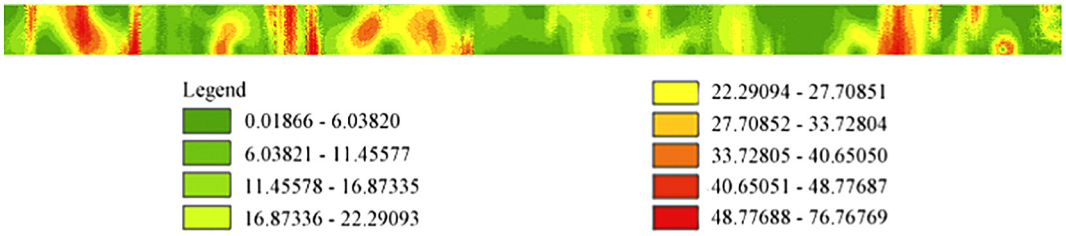

Fig. 11. Slope of top surface of geological body.

suggests that the CK method might be more effective than the IDW method. From the local comparison figure (Fig. 8), we see another advantage of CK method, which is the perfect treatment of the stratal pinch-out phenomenon. In this figure, the red IDW curve shows inconsistent interpolation results with available borehole information because we know that cataclasite strata can only exist when X ≥ 900m. By contrast, the blue CK curve satisfies this requirement, which indicates that the CK technique is capable of dealing with the stratal pinch-out phenomenon while the IDW method cannot. From the point of view of CK estimation evaluation, we did not find any unrealistic or inconsistent places.

We implemented the last two steps of our proposed modeling framework in the ArcGIS and iS3 underground digital platform, which was developed by Tongji University via a mixed programming of Python and C#. The stratum surface TINs were generated by the Arc-scene toolbox and they are shown in Fig. 9. The TINs could be imported into the iS3 platform via 3DS MAX and Unity 3D as transition software. The final 3D geological model in the iS3 platform is presented in Fig. 10; the fault plane is not included in this geological model because of actual geological conditions. In other words, we did not detect any large fault zones around the construction area in this geotechnical engineering project.

Based on the 3D geological model, we were able to obtain a figure of the top surface slope (Fig. 11). In addition, we were able to obtain cross-sectional profiles at any user-defined position; four cross-sectional profiles are shown in Fig. 12, where the letter “w” refers to “weathered”. post-processing

6. Conclusions

This paper presents a collaborative analysis approach for geological body modeling using multi-source geological data and interpolation theories at different stages and at different places. The proposed method is applied to the 3D geological modeling of the Ma-luan mountain tunnel project in Guangdong province, China. The main conclusions are detailed below.

(1) The multi-source data standard for a geological body in a road tunnel engineering project not only normalizes the whole modeling

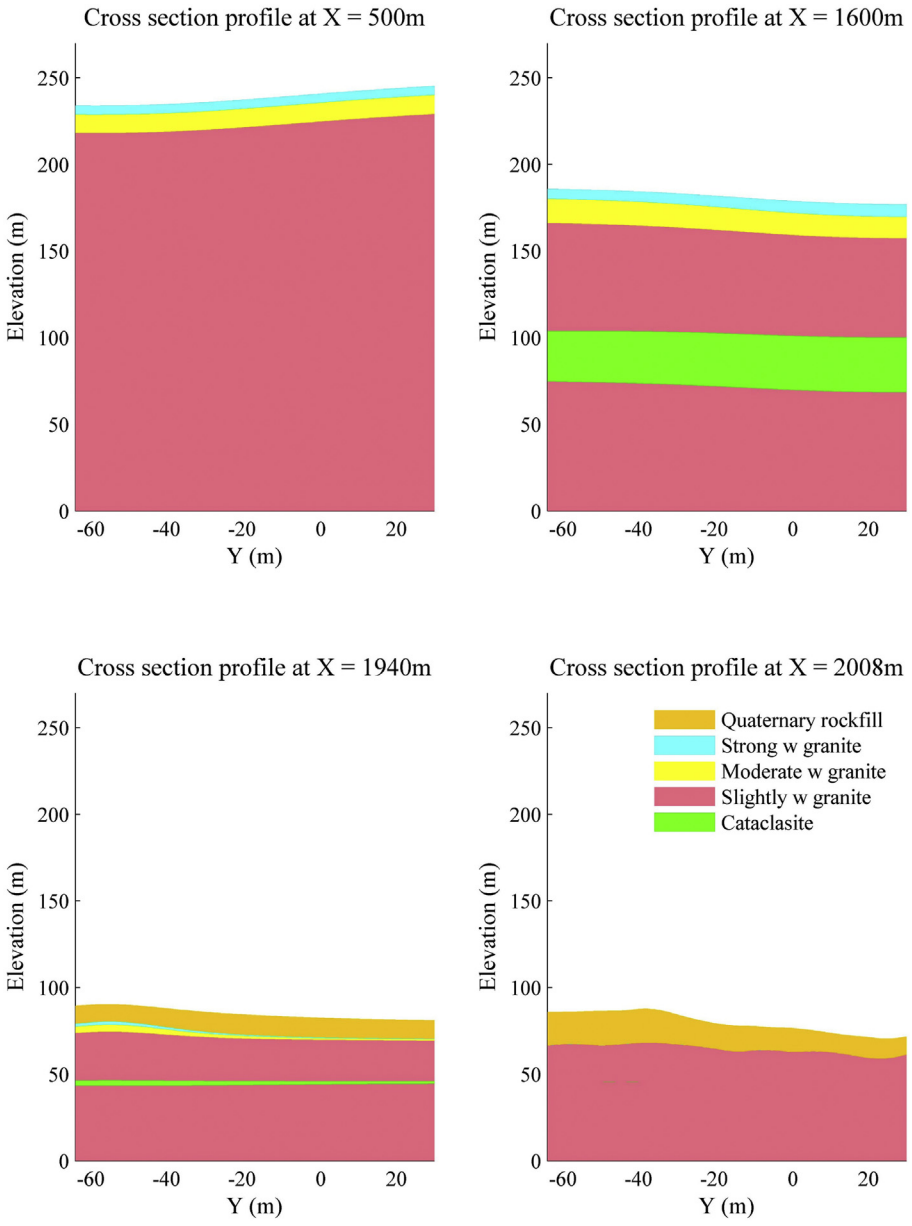

Fig. 12. Transverse cross-section profiles in MATLAB.

process but also makes the data transmission between companies more convenient. In this data standard, we consider both hard and soft data; using the unique ID number, all the data groups are connected systematically and rigorously.

(2) To overcome the limitations of the original borehole data, we adopted the idea of virtual borehole to obtain more information. Of the interpolation methods, the Combined Kriging method shows great advantages over the IDW method because the former can deal with the phenomenon of stratal pinch-out, whereas the latter cannot. This finding is also confirmed by their MSE values of LOOCV, which are $1.3m^2$ and $12.8m^2$, respectively.

(3) In the case of the Ma-luan mountain tunnel project, collaborative modeling analysis can take full advantage of different software to adsorb their strengths and uses iS3 to visualize the 3D model. Given that iS3 is a digital platform for life-cycle analysis of underground infrastructures, the 3D geological model is important in future tunnel construction.

This study provides a basic framework to incorporate multi-source geological data using the proposed data standard; this data can be used to effectively and collaboratively improve the accuracy of 3D models of geological bodies.

Acknowledgments

This work was funded by the National Basic Research Program of China (973 Program: 2011CB013800). The authors gratefully acknowledge the data support from the Tong Yan Civil Engineering Technology Co., Ltd. and software support from the Institute of Tunnel and Underground Engineering – Division No.2, Department of Geotechnical Engineering, College of Civil Engineering, Tongji University. We would like to thank the editor and two anonymous reviewers for their helpful and constructive suggestions for improving the paper.

References

Association of Geotechnical & Geoenvironmental Specialists, 2017. The AGS 4 File Format – Simplicity and Effectiveness. World Wide Web Address. http://www.agsdataformat.com/datatransferv4/intro.php.

buildingSMART, 2015. Open and Neutral Data Format for openBIM (Edition IFC4). World Wide Web Address. http://www.buildingsmart-tech.org/specifications/ifc-releases/ifc4-release/ifc4-release-summary.
Calcagno, P., Chilès, J.P., Courrioux, G., Guillen, A., 2008. Geological modelling from field data and geological knowledge: part I. Modelling method coupling 3D potential-field interpolation and geological rules. Phys. Earth Planet. Inter. 171, 147–157. https://doi.org/10.1016/j.pepi.2008.06.013.
Chang, Y.-S., Park, H.-D., 2004. Development of a web-based Geographic Information System for the management of borehole and geological data. Comput. Geosci. 30, 887–897. https://doi.org/10.1016/j.cageo.2004.07.006.
Chilès, J.-P., Aug, C., Guillen, A., Lees, T., 2004. Modelling the Geometry of Geological Units and its Uncertainty in 3D from Structural Data: The Potential-Field Method. Proceedings of International Symposium on Orebody Modelling and Strategic Mine Planning, Perth, Australia, pp. 24.
Cressie, N., 1985. Fitting variogram models by weighted least squares. J. Int. Assoc. Math. Geol. 17, 563–586. https://doi.org/10.1007/bf01032109.
De Rienzo, F., Oreste, P., Pelizza, S., 2008. Subsurface geological-geotechnical modelling to sustain underground civil planning. Eng. Geol. 96, 187–204.
Devi, M.U., Agarwal, A., Rao, C.R., 2009. Gaussian Variogram Model for Printing Technology Identification. Modelling & Simulation, 2009. AMS'09. Third Asia International Conference on. IEEE, pp. 320–325.
Dong, B., 2013. Research on Geological Modeling and Visualization of Digital Mine. Master Thesis. China University of Geosciences, Beijing, China.
Douaik, A., Van Meirvenne, M., Tóth, T., 2005. Soil salinity mapping using spatio-temporal kriging and Bayesian maximum entropy with interval soft data. Geoderma 128, 234–248.
Fasani, G.B., Bozzano, F., Cardarelli, E., Cercato, M., 2013. Underground cavity investigation within the city of Rome (Italy): a multi-disciplinary approach combining geological and geophysical data. Eng. Geol. 152, 109–121.
Friedman, J.H., 2001. Greedy function approximation: a gradient boosting machine. Ann. Stat. 1189–1232.
Guillen, A., Calcagno, P., Courrioux, G., Joly, A., Ledru, P., 2008. Geological modelling from field data and geological knowledge: part II. Modelling validation using gravity and magnetic data inversion. Phys. Earth Planet. Inter. 171, 158–169.
Hastie, T., Tibshirani, R., Friedman, J.H., 2009. The Elements of Statistical Learning: Data Mining, Inference, and Prediction. Springer.
Holden, L., Mostad, P., Nielsen, B.F., Gjerde, J., Townsend, C., Ottesen, S., 2003. Stochastic structural modeling. Math. Geol. 35, 899–914.
James, G., Witten, D., Hastie, T., Tibshirani, R., 2013. An Introduction to Statistical Learning. Springer.
Jones, T.A., 1988. Modeling geology in three dimensions. Geobyte 3, 14–20 United States.
Kaufmann, O., Martin, T., 2008. 3D geological modelling from boreholes, cross-sections and geological maps, application over former natural gas storages in coal mines. Comput. Geosci. 34, 278–290.
Lam, N.S.-N., 1983. Spatial interpolation methods: a review. Am. Cartogr. 10, 129–150.
Lamorey, G., Jacobson, E., 1995. Estimation of semivariogram parameters and evaluation of the effects of data sparsity. Math. Geol. 27, 327–358. https://doi.org/10.1007/bf02084606.
Lemon, A.M., Jones, N.L., 2003. Building solid models from boreholes and user-defined cross-sections. Comput. Geosci. 29, 547–555.
Li, R., Chen, Y., Dong, F., Qian, L., 1996. 3D data structures and applications in geological subsurface modeling. Int. Arch. Photogr. Remote Sens. 31, 508–513.
Li, X., Wang, C., Zhu, H., 2009. Kriging interpolation and its application to generating stratum model. Rock Soil Mech. 30, 157–162.
Li, X., Li, P., Zhu, H., 2013. Coal seam surface modeling and updating with multi-source data integration using Bayesian Geostatistics. Eng. Geol. 164, 208–221.
Lindsay, M.D., Aillères, L., Jessell, M.W., de Kemp, E.A., Betts, P.G., 2012. Locating and quantifying geological uncertainty in three-dimensional models: analysis of the Gippsland Basin, southeastern Australia. Tectonophysics 546–547, 10–27. https://doi.org/10.1016/j.tecto.2012.04.007.
Liu, Z., Shao, M., Wang, Y., 2013. Large-scale spatial interpolation of soil pH across the Loess Plateau, China. Environ. Earth Sci. 69, 2731–2741. https://doi.org/10.1007/s12665-012-2095-z.
Lu, J., 2002. Systematic identification of polyhedral rock blocks with arbitrary joints and faults. Comput. Geotech. 29, 49–72. https://doi.org/10.1016/S0266-352X(01)00018-0.
Meng, F., 2006. Research on Constructing Way of 3D Stratum Model Based on Drill Data. Master Thesis. Xi'an University of Science and Technology, Xi'an, China.
Oliver, M.A., 2010. The variogram and kriging. In: Handbook of Applied Spatial Analysis, pp. 319–352.
Oliver, M.A., Webster, R., 1990. Kriging: a method of interpolation for geographical information systems. Int. J. Geogr. Inf. Syst. 4, 313–332.
Oliver, M.A., Webster, R., 2015. Geostatistical Prediction: Kriging. Basic Steps in Geostatistics: The Variogram and Kriging. Springer, pp. 43–69.
Sakata, S., Ashida, F., 2011. Integral estimation with the ordinary Kriging method using the Gaussian semivariogram function. Int. J. Numer. Methods Biomed. Eng. 27, 1235–1251.
Shao, Y., Zheng, A., He, Y., Xiao, K., 2011. 3D geological modeling and its application under complex geological conditions. Proc. Eng. 12, 41–46.
Tacher, L., Pomian-Srzednicki, I., Parriaux, A., 2006. Geological uncertainties associated with 3-D subsurface models. Comput. Geosci. 32, 212–221. https://doi.org/10.1016/j.cageo.2005.06.010.
Thierry, P., Prunier-Leparmentier, A.-M., Lembezat, C., Vanoudheusden, E., Vernoux, J.-F., 2009. 3D geological modelling at urban scale and mapping of ground movement susceptibility from gypsum dissolution: the Paris example (France). Eng. Geol. 105, 51–64.
Touch, S., Likitlersuang, S., Pipatpongsa, T., 2014. 3D geological modelling and geotechnical characteristics of Phnom Penh subsoils in Cambodia. Eng. Geol. 178, 58–69. https://doi.org/10.1016/j.enggeo.2014.06.010.
Trangmar, B.B., Yost, R.S., Uehara, G., 1986. Application of geostatistics to spatial studies of soil properties. Adv. Agron. 38, 45–94.
Wang, M., 2004. A Study on Three-Dimensional Geosciences Modeling and Visualization of Engineering Rock Mass. Ph.D Doctoral Thesis. Institute of Rock & Soil Mechanics, The Chinese Academy of Sciences, Wuhan, China.
Wu, Q., Xu, H., 2003. An approach to computer modeling and visualization of geological faults in 3D. Comput. Geosci. 29, 503–509.
Wu, Q., Xu, H., Zou, X., 2005. An effective method for 3D geological modeling with multi-source data integration. Comput. Geosci. 31, 35–43.
Xie, Y., Chen, T.-b., Lei, M., Yang, J., Guo, Q.-j., Song, B., Zhou, X.-y., 2011. Spatial distribution of soil heavy metal pollution estimated by different interpolation methods: accuracy and uncertainty analysis. Chemosphere 82, 468–476.
Xu, H., Wu, Q., Ma, Z., Fei, W., Dong, Q., 2013. A Spatial Data Model and Its Application in 3D Geological Modeling. Fuzzy Systems and Knowledge Discovery (FSKD), 2013 10th International Conference on. IEEE, pp. 903–907.
Zhu, H., Li, X., 2007. Digital underground space and engineering. Chin. J. Rock Mech. Eng. 26, 2277–2288.
Zhu, H., Zheng, G., Wu, J., Ye, W., 2003. Study on ground data model based on drill hole information. J. Tongji Univ. (Nat. Sci.) 31, 535–539.
Zhu, L., Wu, X., Pan, X., 2006. Mechanism and implementation of error correction for 3D strata model. Rock Soil Mech. 27, 268–271.
Zhu, L., Zhang, C., Li, M., Pan, X., Sun, J., 2012. Building 3D solid models of sedimentary stratigraphic systems from borehole data: an automatic method and case studies. Eng. Geol. 127, 1–13.
Zhu, L., Li, M., Li, C., Shang, J., Chen, G., Zhang, B., Wang, X., 2013. Coupled modeling between geological structure fields and property parameter fields in 3D engineering geological space. Eng. Geol. 167, 105–116.